Supporting Information

Voltage Control of Magnetism above Room Temperature in Epitaxial SrCo$_{1-x}$Fe$_x$O$_{3-\delta}$

Shuai Ning[1]*, Qiqi Zhang[2], Connor Occhialini[3], Riccardo Comin[3], Xiaoyan Zhong[2] and

Caroline A. Ross[1]*

This file includes:

Note S1. Magnetism of both BM and P phases of SCO and SFO.

Note S2. Structural evolution of SCFO ($x{\approx}0.5$) with IL gating.

Note S3. STEM images of as-grown and N2G SCFO ($x{\approx}0.5$).

Note S4. RT in-plane coercivity and remanence of 60 nm-thick SCFO ($x{\approx}0.5$).

Note S5. Magnetism of P-SCFO ($x{\approx}0.5$) thin films with different thickness.

Note S6. Structural and magnetic transitions in SCFO ($x{\approx}0.5$) on different substrates.

Note S7. TFY XMCD analysis.

Note S8. Structural evolution of SCFO ($x{\approx}0.5$) with the duration of P2G.

Note S9. Dependence of FM properties on oxygen deficiency in P-SCFO

Note S10. Magnetism switching without topotactic phase transitions.

Note S11. Combinatorial growth of SCFO thin films with varying x.

Note S1. Magnetism of BM and P phases of SCO and SFO.

Both the as-grown SCO and SFO thin films on 001-STO substrate exhibiting the BM crystal structure (Figure S1a, b) have negligible magnetization as indicated by the *M-H* loops measured by VSM at room temperature shown in Figure S1c and d, consistent with the G-type antiferromagnetic ordering in BM phases whose Néel temperature (T_N) is 570 K[1] and 715 K[2] respectively. After IL gating with a voltage of -3 V (denoted as N3G) for 30 mins, both SCO and SFO completely transform to the P phase (Figure S1a, b). No magnetization is observed at RT in the P-SCO produced by N3G.[3] P-SFO (N3G) has no magnetization as it is paramagnetic at RT and has a helical spin structure below the Néel temperature (~134K).[4]
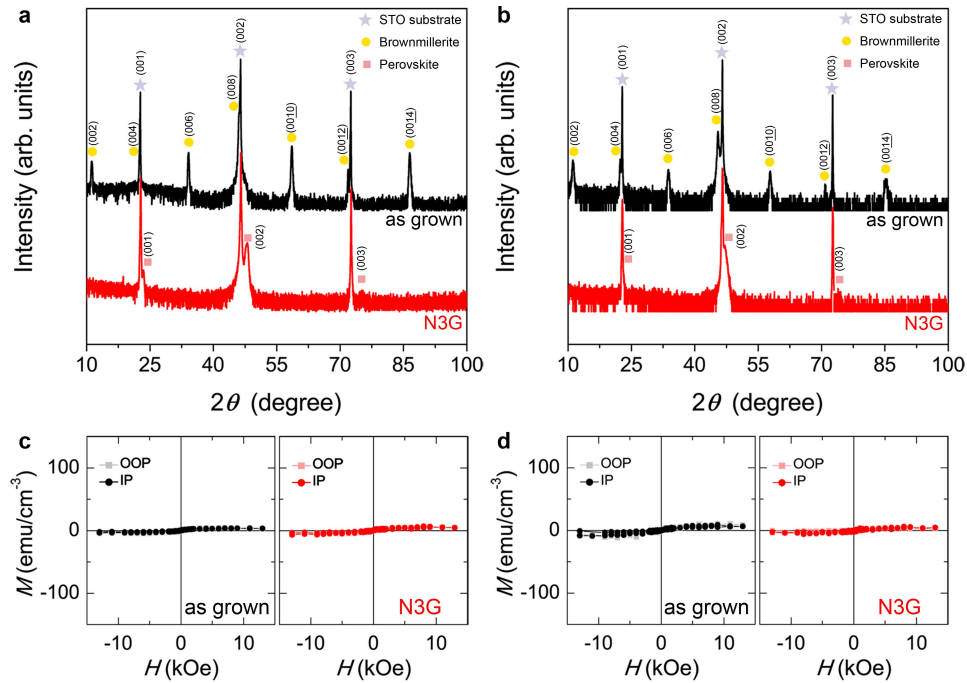

Figure S1. Structure and magnetism of SCO and SFO. (a, b), XRD patterns of as-grown and gated with a voltage of -3 V (N3G) SCO (a) and SFO (b). (c, d), Both in-plane and out-of-plane RT *M-H* loops of as-grown and N3G SCO (c) and SFO (d).

Note S2. Structural evolution of SCFO (*x*≈0.5) with IL gating.

In situ 2*θ*-*ω* XRD measurements were conducted during the IL gating on as-grown BM-SCFO (*x*≈0.5) thin films on STO. The homemade IL gating setup (see Figure S2a) was mounted on the sample holder of XRD instruments. The gating voltage was firstly increased from 0 to -3 V with a step of 0.25 V and an interval of 15 min for each scan. As Figure S2b shows, when the voltage is beyond ~1.5 V, the XRD peak of BM phase shifts towards higher angles indicating a structural change to P phase, and the peak position did not change further with voltage up to -3 V. Figure S2c reveals the structural evolution with reversing the polarity of gating voltage. Upon positive gating, the peak of the P phase gradually shifts towards lower angles, and reaches the BM phase peak position when the voltage is beyond +2 V. With voltages up to +3 V, no change of peak position is found, suggesting no hydrogenation occurs in our experiments.
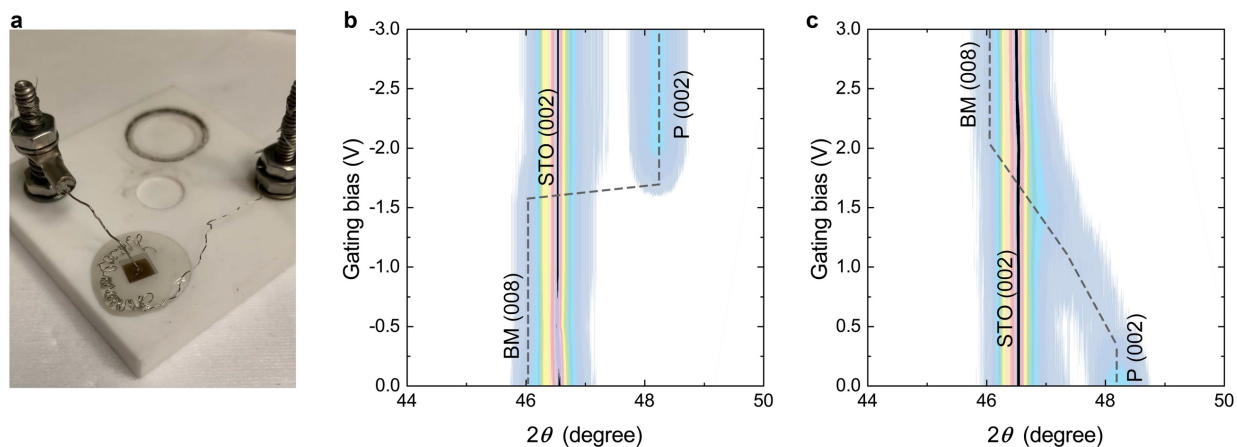

Figure S2. Voltage-dependent *in situ* XRD measurements upon IL gating. (a), photograph of the ionic liquid gating setup, (b), negative gating on the as-grown BM-SCFO (*x*≈0.5) sample, (c), subsequent positive gating on the P-SCFO produced after negative gating.

Note S3. STEM images of as-grown and N2G SCFO ($x \approx 0.5$).

After 30 mins N2G, perovskite phase is observed by HAADF-STEM with in-plane still coherently strained to the STO substrate. Some BM regions are also observed as shown in Figure S3, which is attributed to oxygen loss due to the heating effects during the sputtering of Pt protective layers and ion milling in the TEM specimen preparation process.
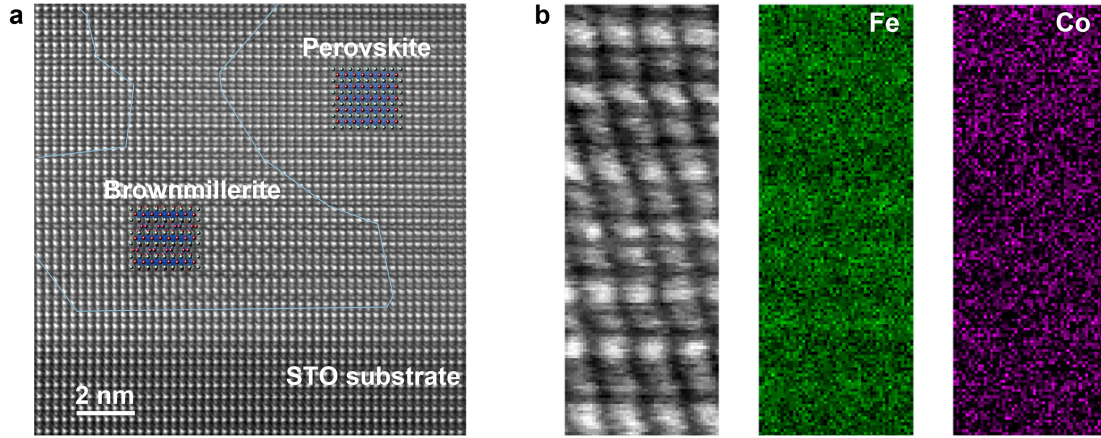

Figure S3. STEM analysis on N2G SCFO ($x \approx 0.5$) thin films. HAADF-STEM image (a) and STEM-EELS mapping (b) taken along the pseudocubic 110-zone axis.

Note S4. RT in-plane coercivity and remanence of 60 nm-thick SCFO ($x \approx 0.5$).

An enlargement of the in-plane *M-H* loop of SCFO ($x \approx 0.5$) thin film after 30 mins N2G is shown in Figure S4. The RT coercivity is ~50 Oe, and the remanence is about 46 emu/cm^3.
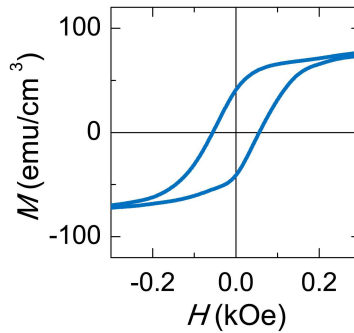

Figure S4. Enlargement of in-plane *M-H* loop of SCFO ($x \approx 0.5$) thin film after 30 mins N2G.

Note S5. Magnetism of P-SCFO ($x \approx 0.5$) thin films with different thickness.

IL gating with a voltage of -2V for 30 mins is able to induce the transitions between BM and P phases in the SCFO ($x \approx 0.5$) thin films with different thickness ranging from 30 to 150 nm. The RT M_S of N2G-yielded P-SCFO ($x \approx 0.5$) films with different thickness are almost same (*i.e.* ~100 emu/cm^3), as shown in Figure S5, indicating the magnetism is an intrinsically volumetric property instead of an interfacial or surface effect.
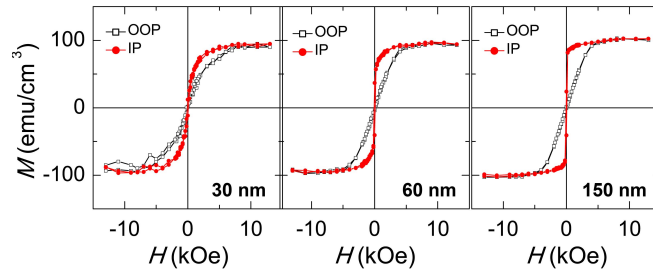

Figure S5. *M-H* loops of SCFO ($x \approx 0.5$) thin films with different thickness. They are measured after 30 mins N2G measured by VSM at room temperature.

Note S6. Structural and magnetic transitions in SCFO on different substrates.

The bulk perovskite SCFO ($x \approx 0.5$) adopts a cubic structure, with a lattice parameter of a=3.844 Å (ICDD 01-082-3347), larger than that of P-SCO (a=3.835 Å, ICDD 01-071-6014) and smaller than that of P-SFO (a=3.851 Å, ICDD 01-070-6802). The brownmillerite SCFO ($x \approx 0.5$) adopts a pseudocubic structure, with lattice parameters a_p=3.934 Å (ICDD 01-084-1685), larger that of BM-SCO (a_p=3.905 Å, ICDD 04-016-2299) but smaller than that of BM-SFO (a_p=3.958 Å, ICDD 01-089-8670). The lattice mismatch of different substrates is listed in Table S1.

As Figure S6a and b show, the as-grown SCFO ($x \approx 0.5$) thin films on both LSAT and LAO substrates exhibit the BM phase with the same oxygen vacancy ordering configuration to that grown on STO substrates. This is analogous to SCO,[5,6] of which the oxygen vacancies favor ordering parallel with the substrate plane within a moderate range from compressive to tensile.

After 30 mins N2G, the peaks assigned to BM phase completely disappear and those of P phase appear. The (013) RSMs shown in Figure S6c and d suggest 30 mins N2G induces complete phase transition from BM to P in the SCFO on both LSAT and LAO, and that the P phases are coherently strained to the substrates. The *M-H* loops of P-SCFO ($x \approx 0.5$) thin films on LSAT and LAO measured after 30 mins N2G (Figure S6e and f) reveal that both of them exhibit FM at RT with an in-plane anisotropy and a M_S of ~100 emu/cm^3, almost the same as that on STO.

Table S1. Epitaxial strain of SCFO with various *x* on different Substrates

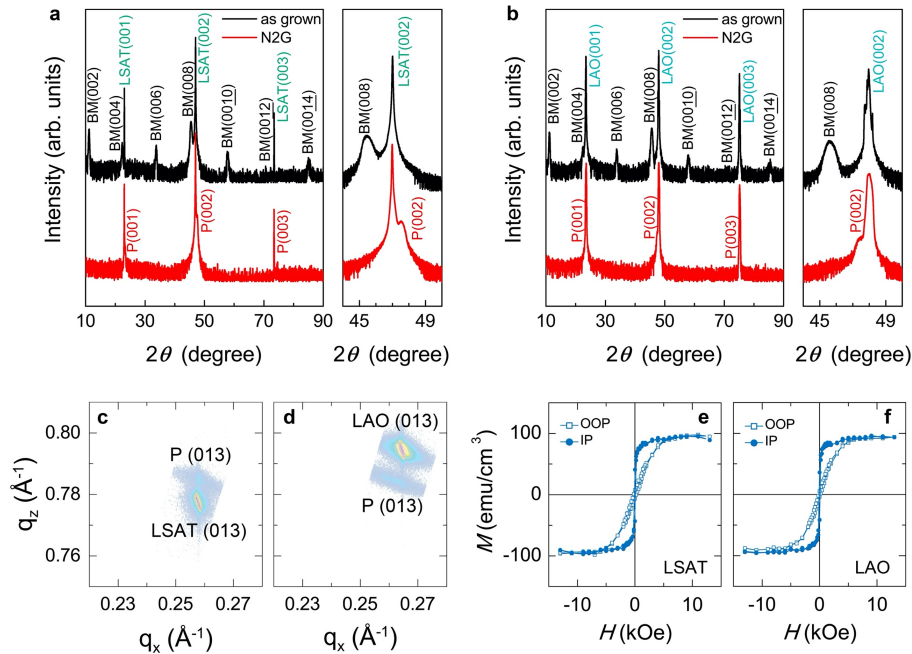| Substrates	Perovskite phase			Brownmillerite phase		
	x=0 a=3.835 Å	x=0.5 a=3.844 Å	x=1 a=3.851 Å	x=0 a_p=3.905 Å	x=0.5 a_p=3.934 Å	x=1 a_p=3.958 Å
STO (3.905 Å)	+1.83%	+1.59%	+1.40%	+0.01%	-0.75%	-1.34%
LSAT (3.868 Å)	+0.86%	+0.62%	+0.44%	-0.94%	-1.68%	-2.29%
LAO (3.788 Å)	-1.22%	-1.46%.	-1.64%	-2.99%	-3.71%	-4.30%

Figure S6. Structure and magnetism of SCFO ($x \approx 0.5$) thin films grown on different substrates. (a, b), the *ex situ* XRD patterns of as-grown and N2G samples on LSAT (a) and LAO (b). (c, d), the *ex situ* RSM around the (013) family of peaks on N2G samples on LSAT (c) and LAO (d). (e, f), RT *M-H* loops of N2G samples on LSAT (e) and LAO (f).

Note S7. TFY XMCD analysis.

X-ray magnetic circular dichroism (XMCD) spectra at Co L-edges, Fe L-edges and O K-edges acquired in total fluorescence mode (TFY) mode (Figure S7) is in agreement with the TEY results.
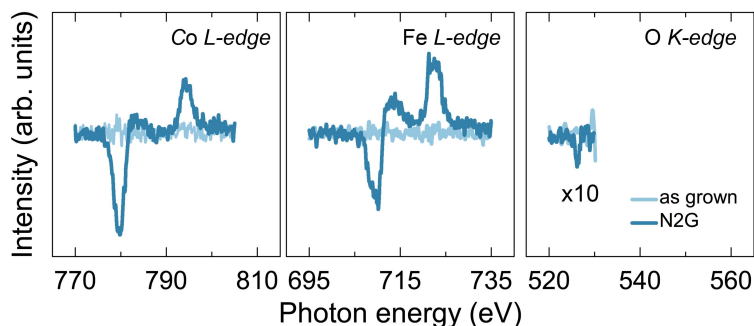
Figure S7. TFY XMCD spectra for both as-grown and N2G SCFO ($x{\approx}0.5$).

Note S8. Structural evolution of SCFO ($x{\approx}0.5$) with the duration of P2G.

The *ex situ* XRD patterns around (002) peak of P-SCFO ($x{\approx}0.5$) on STO produced by 30 mins N2G were measured after 1 min and 3 mins P2G respectively. As shown in Figure S8, slight shifts of the (002) peak of P-SCFO towards lower angle direction are observed with the increase of duration of P2G, indicating that the perovskite structure is still preserved but a small out-of-plane expansion occurs as a number of oxygen vacancies form with the deintercalation of oxygen ions.
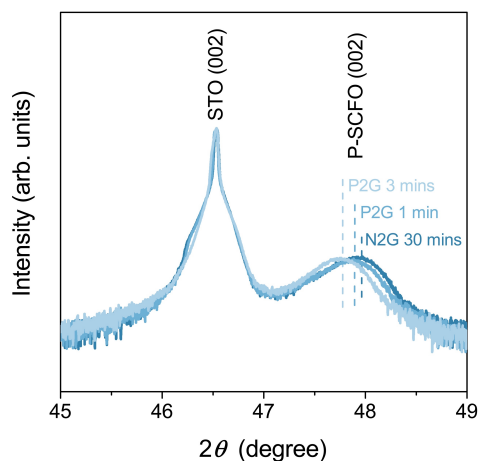
Figure S8. XRD scan evolution of P-SCFO ($x{\approx}0.5$) with duration of P2G.

Note S9. Dependence of FM properties on oxygen deficiency in P-SCFO.

In the end member P-SCO,[3] due to strong hybridization of Co 3d and O 2p orbitals, Co^{4+} ions have intermediate-spin configurations, *i.e.* $t_{2g}^{5-\alpha}e_g^{\alpha}$ or $t_{2g}^{5-\alpha}e_g^{1+\alpha}\underline{L}$ ($0<\alpha\leq1$, $\underline{L}$ denotes a ligand hole). The e_g electrons are accommodated in the itinerant σ^* band, and overlap with the localized t_{2g} band, making the P-SCO a metallic ferromagnet.[7] The other end member, P-SFO, is also metallic, and the Fe^{4+} exhibits high-spin states ($t_{2g}^3e_g^1$ or $t_{2g}^3e_g^2\underline{L}$),[8] which should also favor FM coupling,[9] but the existing long-range Fe-Fe AFM interactions compete with the FM ordering and give rise to a helical spin structure in P-SFO.[4] Increasing δ (by P2G in our work) will add electrons more rapidly to the t_{2g} bands than to the broader e_g bands,[3] lowering the effective magnetic spin number (S) and consequently the T_C according to $T_C = 2zJS(S+1)/3k$ where z is the number of nearest neighbors, J is the exchange constant and k is the Boltzmann constant. Further increasing δ can cause a lattice expansion as shown in Figure S8. The increase of effective Co-Co distance will reduce the hybridization between 2p and 3d orbitals and hence change the crystal field strength. As a result, the Co ions will favor the high-spin state and couple to neighbors antiferromagnetically,[7] thus suppressing the FM coupling.

Note S10. Magnetism switching without topotactic phase transitions.

If the growth is at higher $p(O_2)$ (20 mTorr), we found the as-prepared SCFO ($x\approx0.63$) exhibits a perovskite phase (Figure S9a), qualitatively different from that grown at low $p(O_2)$ (0.1 mTorr) (Figure S10b). This can be due to the fact that Fe^{4+} is more stable than Co^{4+} and hence easier to attain at relatively high $p(O_2)$, which leads to a smaller δ and accounts for the stabilization of P phase in the as-grown SCFO thin films. After 30 mins N2G, as Figure S9a shows, a slight peak

shift toward higher angles is observed, suggesting the as-grown P-SCFO ($x\approx0.63$) is oxygen-deficient and can be further oxidized by N2G while remaining P-phase.

Magnetometry reveals that no magnetization is seen in the as-grown sample despite its P phase, while a typical hysteresis loop appears after 30 mins N2G (Figure S9b). This shows that without a drastic structural phase transition between BM to P, voltage-controlled ON/OFF magnetism can be also realized by tuning the oxygen deficiency in the P-SCFO thin films.
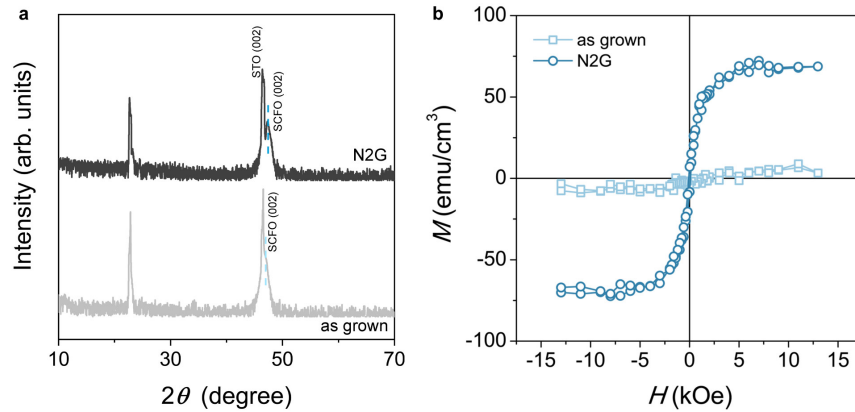

Figure S9. Magnetism switching without topotactic phase transitions. (a), XRD spectra of the SCFO thin films prepared under the $p(O_2)$ of 20 mTorr with $x\approx0.63$ in the as-grown state and after 30 mins N2G. (b), the RT in-plane *M-H* loops of the as-grown and N2G SCFO with $x=0.63$.

Note S11. Combinatorial growth of SCFO thin films with varying *x*.

SCFO thin films with varying x were prepared by combinatorial growth *via* PLD as Figure S10a shows. The growth temperature was 850 °C. During the growth, the SCO and SFO targets were ablated alternately and the substrate holder was rotated 180° each time the targets were switched. The coordinated motion of the substrate holder and targets during growth produced a set of samples with varying *x*. By controlling the ratio of deposition shots between SCO and SFO targets, we can obtain a series of SCFO samples with a full range of *x*.
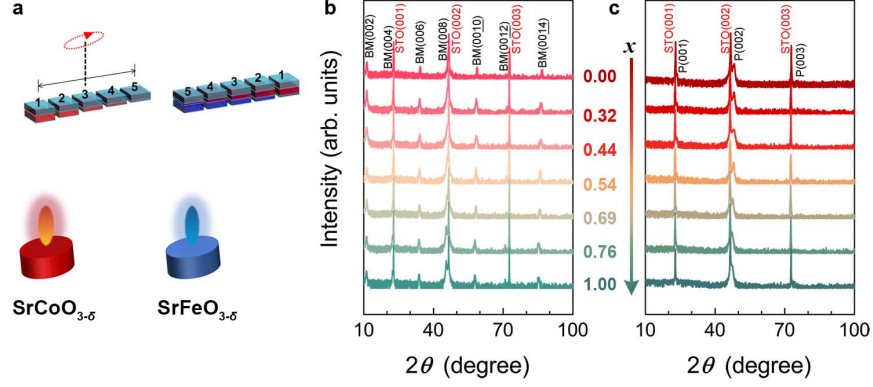
Figure S10. Combinatorial growth of SCFO thin films. (a), schematic of the growth mechanism. (b, c), the full $2\theta\text{-}\omega$ XRD spectra of the SCFO thin films with varying x in the as-grown state (b) and after 30 mins N2G (c).

The oxygen partial pressure, $p(O_2)$, during the combinatorial growth was observed to play a role in determining the structure of the as-grown SCFO thin films. Figure S10b shows that same BM phase structures can be identified for all the as-grown SCFO thin films irrespective of x grown at $p(O_2) = 0.1$ mTorr, and 30 mins N2G induces complete phase transitions from BM to the P phase in all the SCFO thin films with different x (Figure S10c). No RT magnetism is observed in the as-grown SCFO thin films irrespective of x (Figure S11a), while hysteresis loops are observed after 30 mins N2G and the M_S shows a strong dependence on x (Figure S11b), which increases firstly and then decreases with the increase of x.
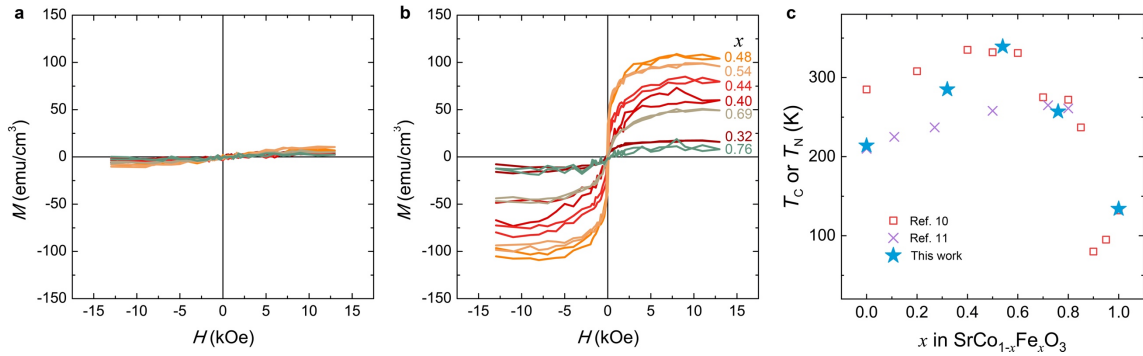

Figure S11. The dependence of magnetism of SCFO thin films on x. (a-b) In-plane $M\text{-}H$ loops measured by VSM at RT of the as-grown state (a) and after 30 mins N2G (b). (c) The Curie temperature of the P-SCFO yielded by 30 mins N2G as a function of the Fe content.

References

(1)   Takeda, T.; Yamaguchi, Y.; Watanabe, H. Magnetic Structure of $SrCoO_{2.5}$. *J. Phys. Soc. Jpn.* **1972,** *33*, 970-972.

(2)   Grenier, J.-C.; Ea, N.; Pouchard, M.; Hagenmuller, P. Structural Transitions at High Temperature in $Sr_2Fe_2O_5$. *J. Solid State Chem.* **1985,** *58*, 243-252.

(3)   Taguchi, H.; Shimada, M.; Koizumi, M. The Effect of Oxygen Vacancy on the Magnetic Properties in The System $SrCoO_{3-\delta}$ ($0 < \delta < 0.5$). *J. Solid State Chem.* **1979,** *29*, 221-225.

(4)   Takeda, T.; Yamaguchi, Y.; Watanabe, H. Magnetic Structure of $SrFeO_3$. *J. Phys. Soc. Jpn.* **1972,** *33*, 967-969.

(5)   Cazorla, C. Lattice Effects on the Formation of Oxygen Vacancies in Perovskite Thin Films. *Phys. Rev. Applied* **2017,** *7*, 044025.

(6)   Hu, S.; Wang, Y.; Cazorla, C.; Seidel, J. Strain-Enhanced Oxygen Dynamics and Redox Reversibility in Topotactic $SrCoO_{3-\delta}$ ($0 < \delta \leq 0.5$). *Chem. Mater.* **2017,** *29*, 708-717.

(7)   Lim, J.; Yu, J. Role of Oxygen Vacancy in The Spin-State Change and Magnetic Ordering in $SrCoO_{3-\delta}$. *Phys. Rev. B* **2018,** *98*, 085106.

(8)   Abbate, M.; Zampieri, G.; Okamoto, J.; Fujimori, A.; Kawasaki, S.; Takano, M. X-Ray Absorption of the Negative Charge-Transfer Material $SrFe_{1-x}Co_xO_3$. *Phys. Rev. B* **2002,** *65*, 165120.

(9)   Takeda, T.; Watanabe, H. Magnetic Properties of the System $SrCo_{1-x}Fe_xO_{3-y}$. *J. Phys. Soc. Jpn.* **1972,** *33*, 973-978.

(10)   Kawasaki, S.; Takano, M.; Takeda, Y. Ferromagnetic Properties of $SrFe_{1-x}Co_xO_3$ Synthesized under High Pressure. *J. Solid State Chem.* **1996,** *121*, 174-180.

(11)   Takeda, T.; Komura, S.; Fujii, H. Magnetic Properties of $SrFe_{1-x}Co_xO_3$. *J. Magn. Magn. Mater.* **1983,** *31-34*, 797-798.